BIOCHEMISTRY
including biophysical chemistry & molecular biology
Article

Biochemistry **2009,** *48,* 4937–4945 4937
DOI: 10.1021/bi9004182

The Cataract-Associated R14C Mutant of Human γD-Crystallin Shows a Variety of Intermolecular Disulfide Cross-Links: A Raman Spectroscopic Study[†,‡]

Ajay Pande, Darnelle Gillot,[§] and Jayanti Pande*

Department of Chemistry, Life Sciences Research Building, University at Albany, State University of New York, Albany, New York 12222. [§]Present address: Mansfield University of Pennsylvania, 31 S. Academy St., Mansfield, PA 16933

Received March 11, 2009; Revised Manuscript Received April 20, 2009

ABSTRACT: The Arg14 to Cys (R14C) mutation in the human γD-crystallin (HGD) gene has been associated with a juvenile-onset hereditary cataract. We showed previously [Pande, A., et al. (2000) *Proc. Natl. Acad. Sci. U.S.A. 97*, 1993−1998] that rapid oxidation of Cys14 in the mutant leads to the formation of intermolecular, disulfide-cross-linked aggregates at physiological pH. Here we present a Raman spectroscopic analysis of R14C and HGD and show that R14C forms such aggregates even at pH 4.5. The lower pH enabled us to monitor the evolution of a variety of disulfide cross-links with distinct conformations around the CC−SS−CC dihedral angles. At least three cysteine residues are involved, forming protein−protein cross-links through disulfide-exchange reactions. From the pattern of the S−S and Trp Raman bands, we infer that Cys32 is likely to be involved in the cross-linking. The data suggest that protein precipitation in the mutant may not be the direct result of disulfide cross-linking, although such cross-linking is the initiating event. Thus, our Raman data not only enhance the understanding of the reactivity of Cys14 in the R14C mutant and the mechanism of opacity, but also shed light on the mechanism of oxidative degradation during long-term storage of thiol-containing pharmaceuticals.

Among the rapidly growing class of inherited cataracts, a sizable number have been associated with mutations in the γ-crystallin genes (*2*, *3*). One such example is the Arg14 to Cys mutation in the HGD[1] gene, observed in juveniles and young adults, and shown to exhibit distinct phenotypes (*4*) (*5*). In this form of hereditary cataract, the lens is clear at birth and gradually develops punctate opacities over a period of time as the affected individual reaches early childhood or young adulthood. Stefan et al. (*4*) were the first to identify the mutation in the HGD gene and speculate, on the basis of molecular modeling alone, about how the mutant protein could lead to the observed cataract.

In a previous publication (*1*), we showed that in contrast to HGD, the R14C mutant rapidly forms protein aggregates composed of intermolecular, disulfide cross-links. More importantly, the R14C mutant forms such aggregates even at protein concentrations that are 2 orders of magnitude lower than that of the wild type. Whereas HGD remains predominantly monomeric and highly soluble up to protein concentrations of 400−500 mg/mL, values typical of crystallin concentrations within the lens fiber cell in vivo (*6*), the R14C mutant forms dimers and higher-order aggregates at concentrations of 1−2 mg/mL at pH 7. Aggregates of R14C eventually become insoluble and precipitate. We concluded that at physiological pH, the molecular basis for the observed light scattering and opacity due to the mutation was the thiol oxidation-mediated protein aggregation triggered by the highly reactive Cys14 residue in R14C. Our results suggested that the thiol group of the surface-localized Cys14 residue (which replaces the solvent-accessible Arg14) was ionized at physiological pH to the thiolate (S^-) form and was extremely reactive, readily forming protein−protein disulfide cross-links. From the extensive cross-linking of R14C, it was evident that in addition to Cys14, at least one other cysteine residue was involved. On the basis of homology modeling, we proposed that the second cysteine residue was likely to be Cys110 (now considered Cys111) with a 10% exposed surface area (*7*). These two cysteine residues acting together could produce the observed pattern of aggregation in the mutant protein.

Besides the dramatic changes observed in the aggregation state, liquid−liquid phase separation behavior, and protein solubility observed in R14C at pH 7 (*1*), another intriguing observation about R14C prompted us to undertake the study presented here. We found that R14C solutions stored at pH 4.5 and 4 °C for several days also showed disulfide-cross-linked aggregates, suggesting a mechanism of thiol-mediated aggregation more complex than what was apparent from our original study.

[†]Supported by NIH Grant EY 10535.
[‡]A preliminary account of this work was presented at the annual meeting of the Association for Research in Vision and Ophthalmology, Ft. Lauderdale, FL, in May 2008.
*To whom correspondence should be addressed. Phone: (518) 591-8842. Fax: (518) 442-3462. E-mail: jpande@albany.edu.
[1]Abbreviations: HGD, recombinant human γD-crystallin protein; R14C, Arg14 to Cys mutant of HGD; BGB, recombinant bovine γB-crystallin protein; DTT, dithiothreitol; DTNB, 5,5′-dithiobis(2-nitrobenzoic acid); HPLC, high-performance liquid chromatography.

Published on Web 04/21/2009

Therefore, we decided to systematically examine the thiol to disulfide conversions in R14C using Raman spectroscopy, which is a proven method for probing the chemical state of protein thiols and disulfide (*8*−*10*). The −SH stretching frequency of cysteine is generally not coupled with any other vibrational mode and typically appears in an isolated region of the Raman spectrum between 2500 and 2600 cm^{-1} (*9*, *10*). The position of the −SH stretch is an indicator of the hydrogen bonding state of the thiol group (*10*, *11*) and thus may reflect its reactivity. The disulfide (S−S) Raman frequency arising from the oxidation of protein thiol groups typically appears in the 500−550 cm^{-1} region at the opposite end of the Raman spectrum, also where there is little overlap with other protein contributions. In model compounds and peptides, some lower-frequency S−S modes below 500 cm^{-1} have also been reported (*12*).

In practical terms, the Raman measurements at pH 7 were problematic because of the ready aggregation of R14C as stated above, and in Pande et al. (*1*). Thus, it was not possible to determine the initial state of the thiol groups (i.e., when all seven Cys residues would be fully protonated) in R14C at physiological pH. Since this was a key first step in tracking the −SH to S−S conversion, we decided to take Raman measurements at pH 4.5 where, as a rule, all seven −SH groups in R14C would be expected to be fully protonated. It should be mentioned that we generally store γ-crystallin solutions at pH 4.5 and 4 °C in sealed and degassed amber-colored ampules for extended periods of time with minimal oxidation and degradation. However, as the Raman data at pH 4.5 show (this report), and contrary to our expectations, we found that the R14C mutant was susceptible to thiol oxidation even at pH 4.5. Furthermore, although the rate of disulfide cross-linking was lower at pH 4.5 than at pH 7, the data reveal the presence of multiple cross-links which probably form via a process of disulfide exchange with neighboring protein molecules. These intermolecular S−S cross-links apparently assume all possible, distinct conformations about the CC−SS−CC torsion angles predicted by other groups based on Raman studies of a number of model disulfides (*13*−*17*). The Raman data also reveal the involvement of at least three and possibly four Cys residues in the oxidation-mediated aggregation of R14C. More importantly, at both pH values (4.5 and 7), the disulfide profiles of the products eventually appear to be identical in the soluble, as well as the insoluble-aggregate phase, suggesting that the final redox status of the cysteine residues in both cases is comparable.

In this study, we attempt to show the potential of Raman spectroscopy in characterizing the thiol oxidation-mediated spectral and phase changes, in a biologically important crystallin mutant. The measurement of the pK_a of Cys14 and other related studies will be published separately.

MATERIALS AND METHODS

Expression and Purification of Recombinant Proteins. All the procedures used here to express, isolate, and purify recombinant wild-type HGD and R14C have been described in detail previously (*1*). Protein solutions that were eluted from the cation-exchange column at pH 4.8 were further dialyzed into 0.275 M sodium acetate buffer (pH 4.5), and concentrated to ~2−5 mM using an extinction coefficient of 41.4 mM^{-1} cm^{-1} at 280 nm for both HGD and R14C (*1*, *18*). For the data at pH 7, protein solutions were dialyzed into 0.1 M sodium phosphate buffer (pH 7.1) (*1*). The purity of the recombinant proteins was checked using electrospray ionization mass spectrometry at the Center for Functional Genomics at the University at Albany. The masses of HGD and R14C so determined were 20608 ± 1 and 20555 ± 1, respectively, which are consistent with our previous determinations for the two proteins (*1*).

Measurement of Thiol Content. The thiol contents of HGD and R14C were determined using the 5,5′-dithiobis(2-nitrobenzoic acid) (DTNB) assay as described in ref *19*. These values agree with those calculated from the areas under the thiol envelopes in the Raman spectra, to within 10%.

Raman Spectroscopy. Raman spectra were measured on a state-of-the-art inVia Raman microscope system from Renishaw Inc. (Gloucestershire, U.K.), equipped with a Leica microscope, an air-cooled CCD detector, and a 785 nm diode laser. Power levels at the sample for 785 nm laser excitation typically averaged ~10 mW. The spectral resolution at this wavelength was 5 cm^{-1}; 10−20 μL of the protein sample at a concentration of 2−5 mM was loaded into quartz capillaries (inside diameter of 1.8 mm) secured on a microscope slide and scanned with 785 nm laser excitation. Since the excitation wavelength is far removed from any protein absorption bands, we did not expect photobleaching or heat-induced sample deterioration effects. However, to ensure sample integrity throughout the measurement, we measured the Raman signal from different spots on the sample by moving the sample stage after every few scans, i.e., signal accumulation for about 10 min. We compared each data set carefully and found no changes in the Raman signals from one data set to another. The individual data sets were then added and processed further. Contributions of buffer bands to the Raman spectra were eliminated using standard subtraction methods. Spectra were calibrated using the 520 cm^{-1} line of silicon. Raman intensities in the −SH region (2500−2800 cm^{-1}) were normalized with respect to a protein band near 2727 cm^{-1} (see the inset of Figure 5) which has been shown to be conformation-insensitive (*11*, *22*). Previous papers have shown this band to appear around 2730−2732 cm^{-1}. Spectra in the lower-frequency region containing S−S bands (495−635 cm^{-1}) and the spectral region typical of protein side chains and secondary structure (700−1700 cm^{-1}) were normalized with respect to the conformation-insensitive phenylalanine bands at 623 and 1003 cm^{-1}, respectively.

Raman spectra of the insoluble aggregates were measured as follows. Aliquots (100 μL) of the sediment from suspensions of R14C samples which were stored at 4 °C for several months, were repeatedly washed with double-distilled water to minimize the concentration of acetate buffer. A 10 μL drop was placed on a glass slide and allowed to evaporate to dryness. Spectra were measured from different points of the sample from 400 to 2800 cm^{-1}, carefully compared and added together, as described above.

Computational Method. To model the effect of a Trp residue located within ~3−4 Å of a disulfide cross-link, we computed the Raman spectra of (a) a tryptophan residue alone, and (b) a cystine together with a tryptophan using density functional theory (DFT) in Guassian 03 (*21*). A B3LYP functional was employed along with the 6-31G (d) basis set to calculate the Raman spectra. Frequencies obtained from the Gaussian calculation were not scaled for comparison with those observed experimentally.

RESULTS

Thiol and Disulfide Spectral Regions. (i) Initial Stages at pH 4.5. In Figure 1A, we compare the Raman spectra of R14C

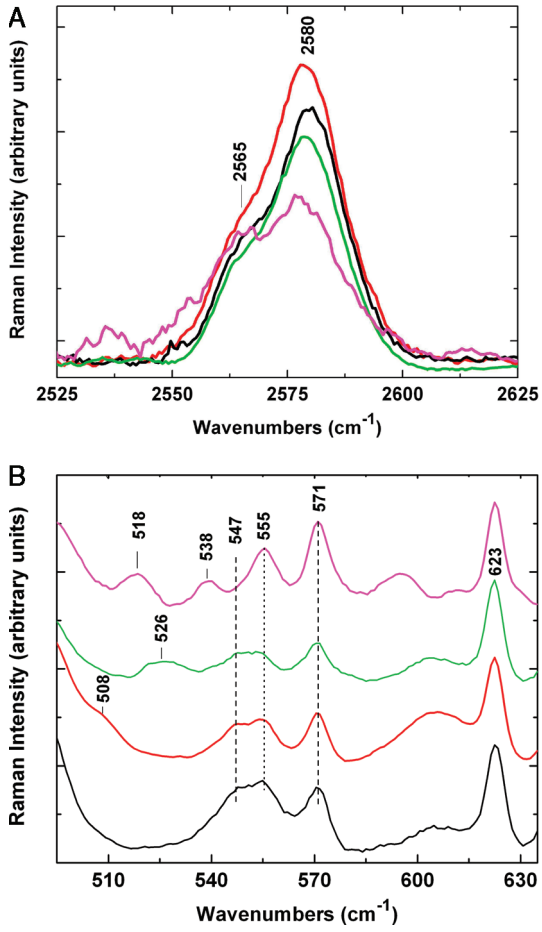

FIGURE 1: Raman spectra of HGD and R14C at pH 4.5 in the (A) −SH frequency region and (B) S−S frequency region: HGD, black curve; freshly prepared R14C, red curve; R14C 48−72 h later, green curve; and R14C several weeks later, pink curve. Intensities in the −SH region are normalized with respect to the conformation-insensitive band at 2727 cm^{-1} (shown in the inset of Figure 5), and in the S−S region with respect to the phenylalanine band at 623 cm^{-1}.

and HGD at pH 4.5, in the 2500−2600 cm^{-1} region typical of the −SH stretching frequency. The corresponding spectra in the S−S frequency region are shown in Figure 1B. The −SH band intensities in Figure 1A are normalized with respect to the conformation-insensitive protein mode at 2727 cm^{-1} [Figure 5 inset (*11*, *22*)].

We now make the assumption that the area under the Raman −SH band of HGD corresponds to six Cys residues, i.e., the total number of Cys residues in HGD, all of which are known to be in the reduced form. The justification for this assumption comes from two sources. (1) We find that in the highly homologous bovine γB-crystallin (BGB), the Raman intensity of each of the seven Cys residues is almost identical, even though the individual −SH frequencies are slightly different (*20*). (2) Raso et al. (*23*) also found that the eight Cys residues in the P22 tail spike protein contribute equally to the composite Raman intensity of the −SH band, even though their individual −SH frequencies were quite distinct. Thus, experimentally, while the precise frequency of the −SH stretching mode depends upon the H-bonding of the −SH group, its Raman cross section appears to be constant.

Figure 1A shows that the −SH bands of R14C and HGD appear as an asymmetric doublet with a main band near 2580 cm^{-1} and a distinct shoulder around 2562−2565 cm^{-1}. In freshly prepared solutions of R14C (red curve), the area under the thiol band envelope corresponds to ∼6.8 cysteine residues relative to HGD (black curve) with 6 cysteine residues. Thus, the ratio of the area of R14C to that of HGD is 6.8/6 or 1.13, which scales closely with 7/6 or 1.17, the ratio of the theoretical number of cysteines in R14C (7 Cys) and HGD (6 Cys). The area under the thiol envelope of R14C is < 10% smaller than the theoretical value, suggesting that the Cys14 thiol is oxidized, albeit minimally, even in freshly prepared solutions.

Within a matter of 48−72 h, the area under the thiol band envelope of R14C (green curve) falls below that of HGD, and the reduced area corresponds to the loss of ∼1.7 ± 0.2 thiol groups. This pattern continues as the samples age further at pH 4.5 such that after several weeks (Figure 1A, pink curve), ∼2.5 ± 0.2 of the seven protein thiols are oxidized. Thus, contrary to expectations, R14C clearly shows thiol oxidation and aggregation also at pH 4.5 in a manner reminiscent of its behavior at pH 7, although at a slower rate.

In Figure 1B, the corresponding spectra in the S−S region for HGD and R14C are shown, with intensities normalized to the phenylalanine band around 623 cm^{-1}. Again, even in freshly prepared solutions (Figure 1B, red curve), the data show a shoulder at 508 cm^{-1}, which is consistent with the small amount of thiol oxidation evident from the −SH region (Figure 1A, red curve), and indicates that disulfide cross-linking has begun. Raman bands near 510 cm^{-1} are typical of disulfide bonds in proteins (*8*, *9*). In parallel, the bands spanning 547−571 cm^{-1} appear to be lower in intensity relative to those of HGD, even though the band profile is essentially unchanged. Within 48−72 h, the 508 cm^{-1} shoulder is replaced by a broad band centered at 526 cm^{-1} (Figure 1B, green curve), which corresponds to the loss of about 1.7 ± 0.2 thiol groups (Figure 1A and previous paragraph). This change is accompanied by a further lowering of intensity in the 547−571 cm^{-1} region. As the sample ages further to several weeks, there is another shift in the pattern of evolution of the S−S frequency (Figure 1B, pink curve). The broad band centered at 526 cm^{-1} (Figure 1B, green curve) is replaced by two disulfide bands centered at 518 and 538 cm^{-1}. Simultaneously, several marked changes occur in the 547−571 cm^{-1} region with a reduction in the intensity of the 547 cm^{-1} band and an increase in the intensity of the 571 cm^{-1} band, and possibly the 555 cm^{-1} band. As mentioned above, although nearly three of the protein thiols are lost in R14C (Figure 1A, pink curve), the aggregates are still largely soluble and reversible to the monomer form with DTT treatment. There is little sedimentation occurring in the solution at this stage.

(ii) Late-Stage Spectra at pH 4.5. The effects of prolonged aging (samples kept at pH 4.5 and 4 °C for several months to a year) are seen in the spectra shown in panels A and B of Figure 2. Here the protein aggregates are no longer soluble and sediment out of solution. Interestingly, we found no further significant change in the Raman spectra of solutions of R14C aged over a year in which the soluble protein coexists with the aggregated protein in the solid phase. A notable feature of these data is that while the −SH region of the soluble (supernatant) phase of R14C shows that approximately half the cysteine residues are oxidized [3.0 ± 0.2 (Figure 2A, red curve)], there is little change in the pattern of evolution of the disulfide bands, or the 547−571 cm^{-1} bands (Figure 2B, red curve) beyond what was observed in Figure 1B (pink curve). The area under the −SH band in the solid aggregates (Figure 2A, green curve) is comparable to that in the supernatant (red curve), but the band profile differs in that it is

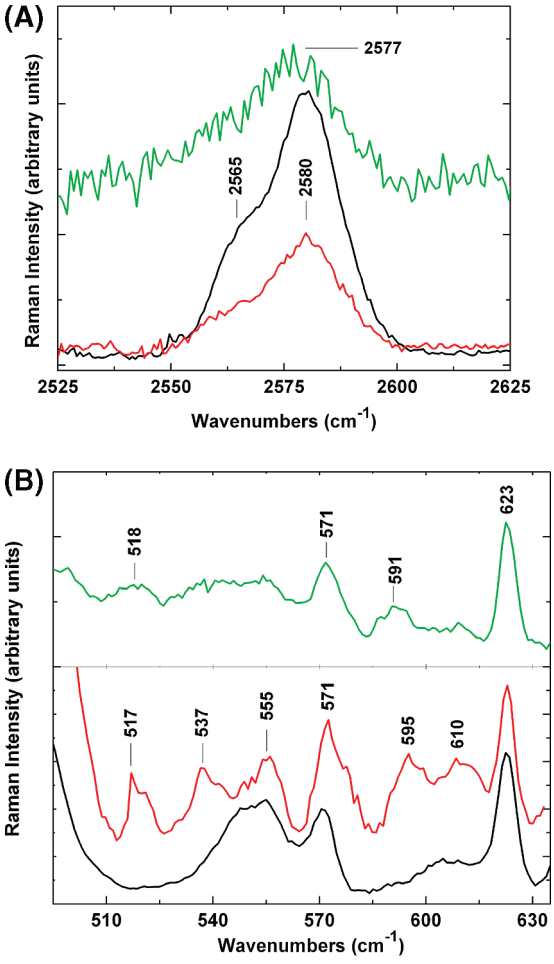

FIGURE 2: Raman spectra of HGD and R14C showing long-term effects at pH 4.5 when insoluble protein aggregates are formed. (A) The −SH region showing no change in HGD (black curve), the R14C supernatant showing that approximately half of the protein thiols remain (red curve), and the solid phase also showing approximately half of the protein thiols remaining (green curve). (B) The S−S region with the same color scheme as in panel A. The overall pattern of disulfides in the supernatant and sediment is nearly identical.

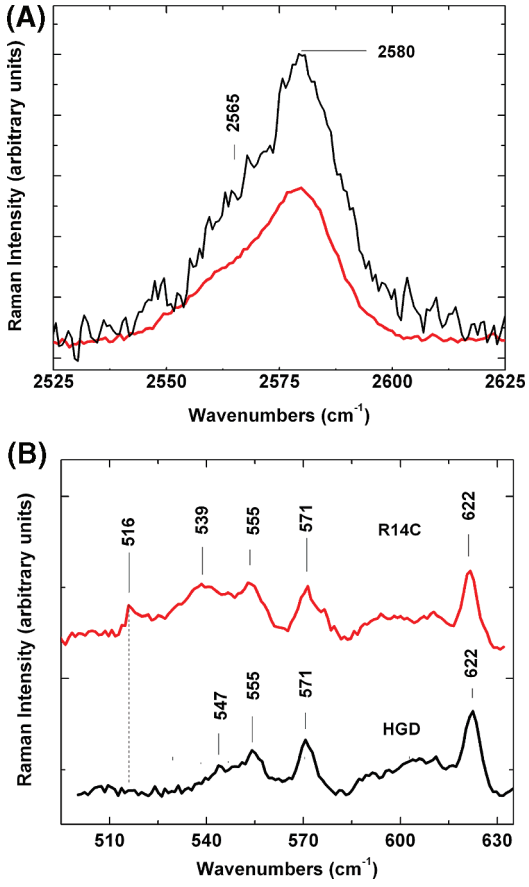

FIGURE 3: Raman spectra of HGD and R14C at pH 7. (A) The −SH region showing freshly prepared HGD (black curve, 6 −SH groups) and R14C in the same time period (red curve, 3.5 ± 0.2 −SH groups). (B) The S−S region for the same samples with the same color scheme.

broader and, unlike that of the supernatant, has no defined shoulder around 2565 cm^{-1}. The data in Figure 2 lead us to conclude that at pH 4.5 about half the cysteine residues of R14C are susceptible to oxidation and intermolecular disulfide cross-linking. Furthermore, protein thiols contributing to both bands in the doublet (2565 and 2580 cm^{-1}) seem to be involved in the aggregation of R14C, with those contributing to 2580 cm^{-1} being preferentially oxidized first. In the disulfide frequency region (Figure 2B, green curve), the sedimented aggregates show a somewhat featureless spectrum, although the S−S frequencies, while rather broad, appear to be at approximately the same location as in the supernatant.

(iii) Spectral Profiles at pH 7. In Figure 3A and 3B we present the Raman spectra in the thiol region and disulfide regions for HGD and R14C at pH 7. At this pH, consistent with our previous observation that R14C undergoes rapid thiol oxidation-mediated aggregation at pH 7 (*1*), we were unable to track the progressive loss of thiols and pattern of evolution of the disulfides which we observed at pH 4.5 (Figures 1 and 2). Thus, the spectrum of R14C shown in Figure 3A (red curve) corresponds to the depletion of approximately half of the protein thiols (3.5 ± 0.2) and is comparable to the data shown in Figure 2A. It is notable that the two spectra of the R14C supernatant (pH 7, Figure 3A, red curve, and pH 4.5, Figure 2A, red curve) are very similar, suggesting that while the rate of oxidation at pH 7 is considerably higher than at pH 4.5, the final redox status of the protein in the two cases is likely to be the same.

(iv) The 545−575 cm^{-1} Region. We noted in the beginning of this section that the emergence of disulfide frequencies in R14C is accompanied by intensity changes in the 547−571 cm^{-1} bands (Figures 1B and 2B). These bands initially show a drop in intensity (Figure 1B, red and green curves), followed by a recovery in the intensity of the 555 and 571 cm^{-1} bands, but not the 547 cm^{-1} band (Figure 1B, pink curve). Raman bands in the 547−571 cm^{-1} region have been shown to arise from some of the numerous ring modes of tryptophan (*24*). Lord and Yu (*25*, *26*) were the first to assign the relatively weak band near 547 cm^{-1} to a tryptophan ring breathing mode in lysozyme and α-chymotrypsin, but not much has been reported about the 547 cm^{-1} band in proteins probably because of overlapping disulfide frequencies in this spectral region. These changes in intensities of the tryptophan ring modes due to disulfide cross-linking suggested a possible interaction between an S−S cross-link and a neighboring Trp residue, and led us to investigate this further. Because of the proximity of Cys32 to Arg14 in the X-ray crystal structure [Figure 4A (*27*)], it seemed probable that an intermolecular disulfide cross-link formed by Cys32 could be involved in such S−S···Trp interactions. We examine this possibility further in the Discussion.

In an attempt to understand the intensity changes in the 547−571 cm^{-1} bands, we modeled the Raman spectra of a

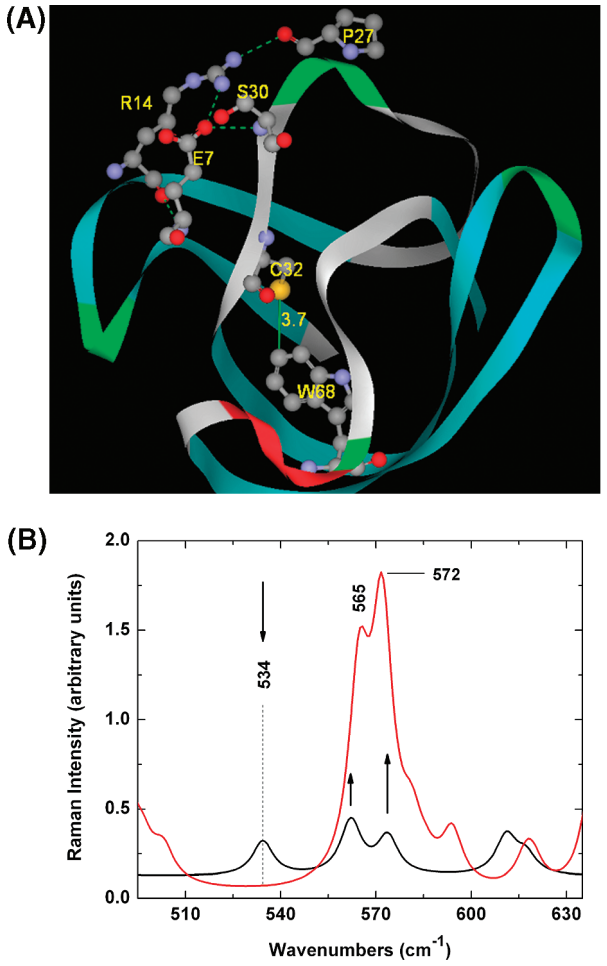

FIGURE 4: (A) Part of the N-terminal domain of HGD (Protein Data Bank entry 1hk0). The proximity of Cys32 and Trp68 is shown (3.7 Å) in the foreground. The extensive H-bonding network of Arg14 with Glu7, Pro27, and Ser30 is indicated in the top left corner. In the R14C mutant, this H-bonding is considerably weakened which in turn may allow Cys32 to be solvent-accessible and amenable to oxidation (see text for details). The picture was drawn using DSViewerPro (Accelrys). (B) Raman spectra of model tryptophan with and without a disulfide bond in the vicinity, generated using Gaussian: tryptophan residue alone (black curve) and tryptophan with a cystine S−S within ~3−4 Å of the indole ring (red curve). The bands at 534, 565, and 572 cm^{-1} closely approximate the bands around 547, 555, and 571 cm^{-1}, respectively, in HGD and R14C which are typically assigned to tryptophan ring modes in proteins.

tryptophan residue alone and a tryptophan residue together with a cystine residue within ~3−4 Å of the S−S bond, using density functional theory implemented in Gaussian 03W (*21*). These results are shown in Figure 4B in which the black curve represents the calculated Raman spectrum for Trp alone and the red curve is the combined Trp plus S−S spectrum. Here we see that a band at 534 cm^{-1} in the spectrum for Trp alone (which is likely to be at 547 cm^{-1} in the protein) is absent in the combined spectrum. At the same time, the intensities of the bands near 565 and 572 cm^{-1} (which are close to the 555 and 571 cm^{-1} bands in R14C) are enhanced in the combined spectrum. We recognize that the calculated model spectra cannot be directly extrapolated to proteins, and the absolute intensities may not be reliable. However, the model spectra do show the same trends in the intensity changes for Trp modes observed in our R14C spectra due to the formation of disulfide cross-links.

−SH Frequency of the Cys14 Thiol Group. From the data in Figure 1A, where thiol oxidation is minimal (red curve), it is possible to determine the −SH frequency of the thiol group of Cys14. In Figure 5, we present the Raman difference spectrum obtained by subtracting the spectrum of HGD from that of R14C (the inset of Figure 5 shows the full spectra in the 2500−2800 cm^{-1} region for HGD and R14C with intensities normalized to that of the 2727 cm^{-1} band). The −SH stretching frequency of Cys14 appears predominantly as a single band centered around 2575 cm^{-1}. A minor conformation may be present as indicated by the shoulder at 2592 cm^{-1}, but given that this shoulder is weak in the difference spectrum, it cannot be identified with certainty. The shift in the Cys14 −SH frequency from 2580 cm^{-1} in R14C to 2575 cm^{-1} indicates that Cys14 is more strongly hydrogen bonded than the cysteine residues contributing to the 2580 cm^{-1} band in R14C. Since Cys14 is located on the protein surface, it is likely to be hydrogen-bonded to either the solvent water or a neighboring H-bond donor.

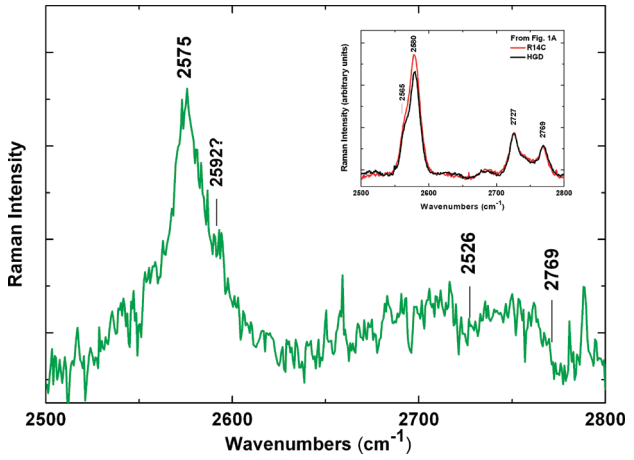

FIGURE 5: Raman difference spectrum of the data shown in Figure 1A showing the −SH frequency of the Cys14 residue in R14C. The inset shows the spectra of HGD and R14C (with minimal thiol oxidation at pH 4.5) used to determine the −SH frequency of the Cys14 residue.

Region Specific to Secondary Structure and Side Chain Modes. Figure 6 shows the Raman spectra of HGD and R14C in the spectral region sensitive to secondary structure and side chain modes. In the 1000−1800 cm^{-1} region (also termed the "fingerprint region"), vibrational modes sensitive to the secondary structure and specific side chains, some of which are conformation-sensitive, are seen. The data show that despite the marked changes in the −SH and S−S stretch regions, bands in the fingerprint region of the mutant protein (red, green, and pink curves) are generally within ±3 cm^{-1} of the those of the wild type (black curve) even in the solid phase containing aggregated protein (pink curve). This includes the amide I and amide III bands at 1672 and 1238 cm^{-1} that are typical of antiparallel β-sheet-containing proteins (*9*), the bands assigned to phenylalanine (623, 1003, and 1032 cm^{-1}) and tyrosine (833, 856, and 1211 cm^{-1}), and the higher-frequency modes of tryptophan (758, 879, and ~1340 cm^{-1}). In proteins, a sharp band near 1360 cm^{-1} which is part of the Fermi doublet consisting of the 1360 and 1340 cm^{-1} bands (*28*) has been assigned to Trp and is reported to be indicative of buried tryptophan residues (*29*). Interestingly, although the Trp residues in HGD are known to be buried (*7*), this band appears only as a weak shoulder in the data shown in Figure 6. The absence of a sharp 1360 cm^{-1} band has also been noted in other proteins in which Trp residues are buried in a hydrophobic environment (*29*). Therefore, contrary to existing beliefs, the 1360 cm^{-1} band may not be a good indicator

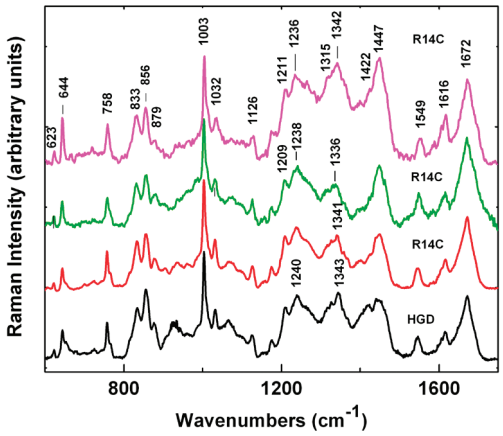

FIGURE 6: Raman spectra of HGD and R14C in the fingerprint region at pH 4.5. Compared to HGD (black curve), the secondary structure of R14C is essentially unchanged in all states of thiol oxidation: R14C solution with little or no oxidation (red curve), R14C solution with less than half the thiols oxidized (green curve), and R14C aggregates in the solid phase with approximately half the thiols oxidized (pink curve). Intensities in this region are normalized with respect to the phenylalanine band at 1003 cm^{-1} but cannot be compared quantitatively for the different samples due to variations in their individual backgrounds.

of the environment of tryptophan residues in proteins. We should state that in this spectral region, due to the varying backgrounds for individual protein samples, changes in peak intensities are not quantitative and cannot be used to identify differences between the two proteins. Nevertheless, the data shown in Figure 6 indicate that the secondary structure of R14C is largely preserved during the various stages of aggregation, including the formation of the solid phase.

DISCUSSION

The Raman spectroscopic data presented here clearly show that the thiol group of Cys14 is sufficiently ionized to the thiolate form not only at physiological pH, consistent with our original conclusion, but also at pH 4.5, which accounts for the formation of disulfide bonds at the lower pH as well. Such aggregation, per se, is not unusual for a cysteine residue located on the protein surface. We have observed a similar pattern of aggregation also in the case of the bovine ortholog, BGB at pH 7, in which the intrinsic Cys15 residue on the surface forms intermolecular, disulfide cross-linked aggregates (*19*). However, what is unusual in the case of R14C is that the Cys14 thiol forms such cross-links also at pH 4.5, a phenomenon not observed in BGB. The Raman frequency assigned to Cys14 in this work (Figure 5) at 2575 cm^{-1} indicates that the reactive −SH group acts as a weak to moderate H-bond donor or acceptor (*10*) either to solvent water or to an internal protein group. Since the three-dimensional structure of R14C is not available, we have modeled the R14C mutation on the HGD structure and find that Glu7 or Tyr28 is the likely residue for H-bonding, depending on the orientation of the −SH group in Cys14. Clearly, the ionization of Cys14 will be influenced by neighboring amino acid residues which could explain why Cys14 is ionized also at the lower pH and may have a pK_a value well below 8.5, the normal pK_a of cysteine. We are in the process of determining the pK_a of Cys14 and will present the data elsewhere.

The Raman data at pH 4.5, obtained by monitoring oxidation-mediated changes over extended periods of time, reveal how the pattern of intermolecular disulfide cross-links evolves in R14C. These changes occur at a faster rate at pH 7; hence, only the final product is seen at this pH. The data at both pH values suggest that at least three or possibly four Cys residues may be involved in the oxidation-mediated aggregation of R14C. The uneven loss in the two −SH bands of R14C as oxidation progresses clearly suggests that the Cys residues contributing to the shoulder around 2565 cm^{-1} (indicative of stronger H-bonding) are much less diminished compared to those contributing to the Cys frequency around 2580 cm^{-1} (which represents a weaker H-bonding of the −SH group). We and others have found that the Raman −SH frequency of individual Cys residues indicates how a single Cys residue can populate two or more distinct hydrogen-bonding states (*20*, *23*). Therefore, it is likely that the −SH group in the Cys residues contributing to the strongly H-bonded state (i.e., the shoulder around 2565 cm^{-1}) is better stabilized and hence less reactive. If that is generally true, the position of the Raman SH band may become a good indicator of its reactivity. On the basis of our high-resolution X-ray crystal structure of HGD (*27*), we previously invoked the participation of the partially exposed Cys110 (now designated as Cys111) in addition to Cys14 in intermolecular disulfide cross-linking and aggregation (*1*). In addition, we now suggest that Cys32, in the N-terminal domain, which is not solvent-accessible in HGD (*7*) may also be implicated in intermolecular cross-linking together with Cys14 and Cys111.

The X-ray crystal structure of HGD (*27*) shows two domains of almost equal size, each consisting of two Greek key motifs. In HGD, Arg14 is extensively H-bonded to Pro27, Tyr28, and Ser30 and may play a role in maintaining the local structure in the first Greek key motif. Replacement of Arg14 with Cys clearly results in a diminution of this H-bonding network since Cys14 cannot form all these H-bonds. The overall effect of weakened H-bonding may be an increased flexibility of the local structure surrounding residue 14. Thus, the long loop (residues 19−33) containing Cys32 is less constrained, making the Cys32 thiol solvent-accessible and amenable for intermolecular disulfide formation (Figure 4A). Such a disulfide bond would be <4 Å from Trp68. It should be noted that Cys78 and Trp42 are also ~4 Å apart, but that region of the structure in R14C is more distant and not likely to be affected by the mutation at residue 14. Thus, from our previously published HPLC data (*1*), which showed that progressively larger disulfide-linked aggregates form in solutions of R14C over time, and our current data which show that as oxidation progresses, there is an inverse correlation between the intensities of the S−S Raman bands with a Trp Raman band (Figure 1B), we conclude that Cys32 is likely to be involved in intermolecular disulfide cross-linking. While an intramolecular S−S bond involving Cys18 and Cys78, which would be close to Trp42, is possible, we reject this possibility since it cannot explain the formation of progressively larger aggregates over time. Furthermore, Hains and Truscott (*30*) report that Cys18 remains in the reduced form even in very advanced cases of nuclear cataract in which all other Cys residues appear to be oxidized. Hence, intramolecular S−S cross-linking involving Cys18 is highly unlikely. Finally, we recognize that the unambiguous identification of intermolecular disulfides would require other analytical techniques such as mass spectrometric analysis of peptides derived from the cross-linked products. That type of analysis is, however, beyond the scope of this work.

For the assignment of Raman bands between 547 and 571 cm^{-1}, we defer to the work of two groups of investigators

who have assigned experimentally (*24*) and theoretically (*31*) several Raman bands of indole and tryptophan, including those around 544, 554, and 571 cm^{-1}, to indole ring deformation modes. From their work, we conclude that the Raman band near 540 cm^{-1}, in HGD and R14C, most likely arises from a benzene ring deformation mode in tryptophan. Our calculated spectra of a tryptophan residue with and without a cystine disulfide bridge within 3−4 Å of the indole ring (Figure 4B) show that the Trp ring mode at 534 cm^{-1} is absent when coupled with an S−S linkage in its vicinity, even as the bands at 565 and 572 cm^{-1} are considerably enhanced.

Interactions such as those described above between aromatic rings and disulfides are quite common in proteins and are often invoked to understand their biological function. In a recent review of such interactions, Meyer et al. (*32*) highlight the finding (*33*) that in a survey of more than 60 structures of immunoglobulin (Ig) proteins, a highly conserved (Cys SS)···Trp interaction emerges within the Ig fold motif. Clearly, therefore, such Trp−disulfide interactions are biologically important, and Raman spectroscopy may be a good technique for detecting them. In fact, ultraviolet (UV) resonance Raman spectroscopy with an excitation wavelength close to 280 nm (the absorption maximum of tryptophan) may be a better tool for identifying such interactions definitively; however, so far, the UV resonance Raman studies of Trp have focused only on the tryptophan Raman lines above 700 cm^{-1} (*34*), and to the best of our knowledge, no data are currently available in the lower-frequency region.

Conformations of Disulfides. Our Raman data also reveal an intriguing variety of disulfide cross-links. The first discernible S−S band at 508 cm^{-1} appears as a small shoulder at the onset of aggregation in R14C when the concentration of aggregates detected by HPLC is minimal (≤3%). An S−S frequency around 510 cm^{-1} has been routinely observed in proteins containing intramolecular disulfide bonds arising from cystine residues (*9*). For R14C, however, this band seems to be an indicator of an intermolecular S−S cross-link at the early stage of protein aggregation. Wild-type HGD does not have cystine residues, and no intramolecular S−S bonds have been detected (*27*). The disappearance of this band and the emergence of a broad S−S band near 526 cm^{-1} as aggregation proceeds further suggest that disulfide-exchange reactions and rearrangements between neighboring protein molecules may be taking place until stable and distinct disulfide frequencies emerge around 518 and 538 cm^{-1}, both in the soluble protein and in the solid phase (Figures 1B and 2B).

On the basis of a comprehensive examination of model compounds containing a variety of primary, secondary, and tertiary disulfide bonds, Sugeta et al. (*13*, *14*) and van Wart and Scheraga (*15*, *16*) have correlated the observed S−S stretching frequencies in the Raman spectra to the conformation of the CC−SS−CC moieties in these compounds. Their work collectively suggests that in the case of primary disulfides (such as cystine), (a) a ν(S−S) around 510 ± 5 cm^{-1} arises from a gauche−gauche−gauche conformation or a dihedral angle, χ(SS−CC), between 50° and 180° on either side of the S−S bond, (b) a ν(S−S) of 525 ± 5 cm^{-1} has a trans−gauche−gauche conformation or a χ(SS−CC) of 0−50° and 50−180° on either side, and (c) a ν(S−S) near 540 ± 5 cm^{-1} has a trans−gauche−trans conformation or a χ(SS−CC) of 0−50° (*13*, *14*, *17*). These assignments have generally been applied to proteins containing intramolecular disulfides but have recently been used to interpret the intermolecular disulfide frequencies in the Raman spectra of peptides of a lung surfactant (*12*). Our data show that in R14C, the conformations of the intermolecular, primary disulfide cross-links in the 500−540 cm^{-1} region fall mainly into these three recognized classes.

It should be mentioned that for R14C, we have observed what appear to be additional disulfide bands below 500 cm^{-1} that are not present in HGD (data not shown). These bands are not shown because they are superimposed on a broad, moderately intense protein mode of unknown origin in HGD around 490−496 cm^{-1} (*35*) which makes it difficult to accurately detect and assign them. However, their presence suggests that disulfide conformations with strained S−S bonds as originally suggested by van Wart and Scheraga (*16*) may be formed during protein−protein disulfide cross-linking in R14C. Strained disulfides have also been reported in lung surfactant peptides by Biswas et al. (*12*).

Aggregation and Overall Protein Structure. The Raman data shown here also support our view that global protein unfolding is not required to effect the pathological changes due to a point mutation in proteins (*1*). Even at advanced stages of thiol oxidation, the secondary structure of the mutant protein is maintained. Li et al. (*36*) have studied the effect of intermolecular disulfide bond formation on the structure and stability of a member of the TGF-β family of proteins, and shown that these characteristics are not altered by intermolecular disulfide cross-linking. To the best of our knowledge, the Raman data presented here are the first to reveal that multiple conformational isomers of intermolecular disulfide cross-links are formed by disulfide-exchange reactions in a disease-associated mutant of human γD-crystallin. In an interesting study using Raman spectroscopy, Schlucker et al. (*37*) have also identified conformational isomers of protein disulfides due to a disease-linked genetic mutation in hair shafts.

As shown in Results, only approximately half of the cysteine residues in R14C are involved in intermolecular disulfide cross-linking in both solution and solid phases. Thus, the aggregation of R14C to the insoluble phase must proceed by secondary mechanisms following disulfide cross-linking. Previously (*1*), we observed the temporal evolution of aggregation in dilute (1−2 mg/mL) solutions of R14C at neutral pH and found that dimers and higher-order oligomers are formed that could be quantitatively reversed to monomers with DTT. However, when the protein concentration was higher than ∼100 mg/mL, the initially formed soluble oligomers rapidly lead to protein precipitation, but the precipitate could not be quantitatively monomerized with DTT. Therefore, at high protein concentrations, protein precipitation is likely to result from a mechanism other than disulfide cross-linking even though it is initiated by such cross-linking. On the basis of these observations, it is tempting to suggest a mechanism for the observed irreversible aggregation, which is similar to the one put forth by Guo and Eisenberg (*38*) for amyloid formation in which intermolecular disulfide cross-links facilitate "runaway domain swapping". As the name implies, it is distinct from the domain swapping which leads to homologous dimer formation in some proteins, such as in βB2-crystallin, a member of the β-γ-crystallin family (*39*). Cho et al. (*40*) have looked into a large number of cases of domain swapping in a variety of proteins and have provided an interesting computational analysis of this process, especially the involvement of disulfide bonds. Their results suggest that intermolecular disulfide bonds may be critical to facilitating domain swapping in some proteins.

Implications for Pharmaceutical Applications and Cataract Formation in Vivo. Our Raman data also highlight how the long-term storage of protein solutions often leads to oxidation and disulfide cross-link formation. Such oxidation-mediated changes caused by the aging of protein solutions are an important challenge for the pharmaceutical industry as well (*41*, *42*), where it is essential that protein-based drugs stored for long periods of time remain viable. Our studies suggest that Raman spectroscopy can be a useful technique for tracking and quantifying the evolution of disulfide cross-links over time, in both the solution and solid phases of protein-based drugs.

The observation that aggregation of R14C can be suppressed by DTT in the early stages (ref *1* and this report) clearly suggests that the deleterious effects of this mutation can be inhibited under reducing conditions. Since the lens is known to have strong redox regulation mediated by several enzymes, including thiol transferase and thioredoxin (*43*), it is rather puzzling that individuals with this mutation do suffer from cataracts, although the progression of opacity appears to vary with the individual even within a family (*4*). This suggests the possibility that the redox systems may be compromised to different degrees in these individuals. The recent work of Lofgren et al. (*44*) shows that in thiol transferase knockout mice, the susceptibility of lens epithelial cells to oxidative stress is significantly enhanced. It is conceivable that the reduced level of redox regulating enzymes in these individuals may affect the progression of the cataract. We propose that the levels of redox regulating enzymes in the cataractous lens materials from affected individuals be carefully compared, which would be an important step toward providing a plausible mechanism of cataract formation in vivo due to this mutation.

ACKNOWLEDGMENT

D.G. gratefully acknowledges the University at Albany Summer Research Program for the opportunity to participate in research in the Pande laboratory.

REFERENCES

1. Pande, A., Pande, J., Asherie, N., Lomakin, A., Ogun, O., King, J. A., Lubsen, N. H., Walton, D., and Benedek, G. B. (2000) Molecular basis of a progressive juvenile-onset hereditary cataract. *Proc. Natl. Acad. Sci. U.S.A. 97*, 1993–1998.
2. Shiels, A., and Hejtmancik, J. F. (2007) Genetic Origins of Cataract. *Arch. Ophthalmol. 125*, 165–173.
3. Andley, U. P. (2007) Crystallins in the eye: Function and pathology. *Prog. Retinal Eye Res. 26*, 78–98.
4. Stephan, D. A., Gillanders, E., Vanderveen, D., Freas-Lutz, D., Wistow, G., Baxevanis, A. D., Robbins, C. M., VanAuken, A., Quesenberry, M. I., Bailey-Wilson, J., Juo, S. H., Trent, J. M., Smith, L., and Brownstein, M. J. (1999) Progressive juvenile-onset punctate cataracts caused by mutation of the γD-crystallin gene. *Proc. Natl. Acad. Sci. U.S.A. 96*, 1008–1012.
5. Gu, F., Li, R., Ma, X. X., Shi, L. S., Huang, S. Z., and Ma, X. (2006) A missense mutation in the γD-crystallin gene CRYGD associated with autosomal dominant congenital cataract in a Chinese family. *Mol. Vision 12*, 26–31.
6. Jaffe, N. S., and Horwitz, J. (1992) *Lens and Cataract*, Vol. *3*, Gower, New York.
7. Srikanthan, D., Bateman, O. A., Purkiss, A. G., and Slingsby, C. (2004) Sulfur in human crystallins. *Exp. Eye Res. 79*, 823–831.
8. Parker, F. S. (1983) *Applications of infrared, Raman, and resonance Raman spectroscopy in biochemistry*, Plenum, New York.
9. Tu, A. T. (1986) in *Spectroscopy of Biological Systems* (Clark, R. J. H., and Hester, R. E., Eds.) pp 47−111, John Wiley & Sone Ltd., New York.
10. Miura, T., and Thomas, G. J. Jr. (1995) Raman spectroscopy of proteins and their assemblies. *Subcell. Biochem. 24*, 55–99.
11. Ozaki, Y., Mizuno, A., Itoh, K., and Iriyama, K. (1987) Inter- and intramolecular disulfide bond formation and related structural changes in the lens proteins. A Raman spectroscopic study in vivo of lens aging. *J. Biol. Chem. 262*, 15545–15551.
12. Biswas, N., Waring, A. J., Walther, F. J., and Dluhy, R. A. (2007) Structure and conformation of the disulfide bond in dimeric lung surfactant peptides SP-B1-25 and SP-B8-25. *Biochim. Biophys. Acta 1768*, 1070–1082.
13. Sugeta, H., Go, A., and Miyazawa, T. (1972) S-S- and C-S stretching vibrations and molecular conformations of dialkyl disulfides and cystine. *Chem. Lett.*, 83–86.
14. Sugeta, H., Go, A., and Miyazawa, T. (1973) Vibrational spectra and molecular conformations of dialkyl disulfides. *Bull. Chem. Soc. Jpn. 46*, 3407–3411.
15. Van Wart, H. E., and Scheraga, H. A. (1976) Raman spectra of strained disulfides. Effect of rotation about sulfur-sulfur bonds on sulfur-sulfur stretching frequencies. *J. Phys. Chem. 80*, 1823–1832.
16. Van Wart, H. E., and Scheraga, H. A. (1976) Raman spectra of cystine-related disulfides. Effect of rotational isomerism about carbon-sulfur bonds on sulfur-sulfur stretching frequencies. *J. Phys. Chem. 80*, 1812–1823.
17. Van Wart, H. E., and Scheraga, H. A. (1986) Agreement with the disulfide stretching frequency-conformation correlation of Sugeta, Go, and Miyazawa. *Proc. Natl. Acad. Sci. U.S.A. 83*, 3064–3067.
18. Andley, U. P., Mathur, S., Griest, T. A., and Petrash, J. M. (1996) Cloning, expression, and chaperone-like activity of human αA-crystallin. *J. Biol. Chem. 271*, 31973–31980.
19. Pande, J., Lomakin, A., Fine, B., Ogun, O., Sokolinski, I., and Benedek, G. (1995) Oxidation of γII-crystallin solutions yields dimers with a high phase separation temperature. *Proc. Natl. Acad. Sci. U.S.A. 92*, 1067–1071.
20. Pande, J., and Pande, A. (2002) The Sulfhydryls of the γ-Crystallins: A Vibrational Spectroscopic Analysis. *Invest. Ophthalmol. Visual Sci. 186*, (Abstract 4660).
21. Frisch, M. J., Trucks, G. W., Schlegel, H. B., Scuseria, G. E., Robb, M. A., Cheeseman, J. R., Montgomery, J. A., Jr., Vreven, T., Kudin, K. N., Burant, J. C., Millam, J. M., Iyengar, S. S., Tomasi, J., Barone, V., Mennucci, B., Cossi, M., Scalmani, G., Rega, N., Petersson, G. A., Nakatsuji, H., Hada, M., Ehara, M., Toyota, K., Fukuda, R., Hasegawa, J., Ishida, M., Nakajima, T., Honda, Y., Kitao, O., Nakai, H., Klene, M., Li, X., Knox, J. E., Hratchian, H. P., Cross, J. B., Bakken, V., Adamo, C., Jaramillo, J., Gomperts, R., Stratmann, R. E., Yazyev, O., Austin, A. J., Cammi, R., Pomelli, C., Ochterski, J. W., Ayala, P. Y., Morokuma, K., Voth, G. A., Salvador, P., Dannenberg, J. J., Zakrzewski, V. G., Dapprich, S., Daniels, A. D., Strain, M. C., Farkas, O., Malick, D. K., Rabuck, A. D., Raghavachari, K., Foresman, J. B., Ortiz, J. V., Cui, Q., Baboul, A. G., Clifford, S., Cioslowski, J., Stefanov, B. B., Liu, G., Liashenko, A., Piskorz, P., Komaromi, I., Martin, R. L., Fox, D. J., Keith, T., Al-Laham, M. A., Peng, C. Y., Nanayakkara, A., Challacombe, M., Gill, P. M. W., Johnson, B., Chen, W., Wong, M. W., Gonzalez, C., and Pople, J. A. (2004) *Gaussian 03*, Gaussian, Inc, Wallingford, CT.
22. Pande, J., Hanlon, E., and Pande, A. (2002) A comparison of the environment of thiol groups in bovine and human γ crystallins using Raman spectroscopy. *Exp. Eye Res. 75*, 359–363.
23. Raso, S. W., Clark, P. L., Haase-Pettingell, C., King, J., and Thomas, G. J. Jr. (2001) Distinct cysteine sulfhydryl environments detected by analysis of Raman S-H markers of Cys → Ser mutant proteins. *J. Mol. Biol. 307*, 899–911.
24. Hirakawa, A. Y., Nishimura, Y., Matsumoto, T., Nakanishi, M., and Tsuboi, M. (1978) Characterization of a Few Raman Lines of Tryptophan. *J. Raman Spectrosc. 7*, 282–287.
25. Lord, R. C., and Yu, N. T. (1970) Laser-excited Raman spectroscopy of biomolecules. I. Native lysozyme and its constituent amino acids. *J. Mol. Biol. 50*, 509–524.
26. Lord, R. C., and Yu, N. T. (1970) Laser-excited Raman spectroscopy of biomolecules. II. Native ribonuclease and α-chymotrypsin. *J. Mol. Biol. 51*, 203–213.
27. Basak, A., Bateman, O., Slingsby, C., Pande, A., Asherie, N., Ogun, O., Benedek, G. B., and Pande, J. (2003) High-resolution X-ray crystal structures of human γD crystallin (1.25 Å) and the R58H mutant (1.15 Å) associated with aculeiform cataract. *J. Mol. Biol. 328*, 1137–1147.
28. Harada, I., Miura, T., and Takeuchi, H. (1986) Origin of the doublet at 1360 and 1340 cm^{-1} in the Raman-spectra of tryptophan and related compounds. *Spectrochim. Acta, Part A 42*, 307–312.
29. Miura, T., Takeuchi, H., and Harada, I. (1988) Characterization of individual tryptophan side chains in proteins using Raman

spectroscopy and hydrogen-deuterium exchange kinetics. *Biochemistry 27*, 88–94.
30. Hains, P. G., and Truscott, R. J. (2008) Proteomic analysis of the oxidation of cysteine residues in human age-related nuclear cataract lenses. *Biochim. Biophys. Acta 1784*, 1959–1964.
31. Majoube, M., and Vergoten, G. (1992) Vibrational Spectra of Indole and Assignments on the Basis of Ab Initio Force Fields. *J. Raman Spectrosc. 23*, 431–444.
32. Meyer, E. A., Castellano, R. K., and Diederich, F. (2003) Interactions with aromatic rings in chemical and biological recognition. *Angew. Chem., Int. Ed. 42*, 1210–1250.
33. Ioerger, T. R., Du, C., and Linthicum, D. S. (1999) Conservation of Cys-Cys Trp structural triads and their geometry in the protein domains of immunoglobulin superfamily members. *Mol. Immunol. 36*, 373–386.
34. Takeuchi, H. (2003) Raman structural markers of tryptophan and histidine side chains in proteins. *Biopolymers 72*, 305–317.
35. Yu, N. T., and East, E. J. (1975) Laser Raman spectroscopic studies of ocular lens and its isolated protein fractions. *J. Biol. Chem. 250*, 2196–2202.
36. Li, T., Yamane, H., Arakawa, T., Narhi, L. O., and Philo, J. (2002) Effect of the intermolecular disulfide bond on the conformation and stability of glial cell line-derived neurotrophic factor. *Protein Eng. 15*, 59–64.
37. Schlucker, S., Liang, C., Strehle, K. R., DiGiovanna, J. J., Kraemer, K. H., and Levin, I. W. (2006) Conformational differences in protein disulfide linkages between normal hair and hair from subjects with trichothiodystrophy: A quantitative analysis by Raman microspectroscopy. *Biopolymers 82*, 615–622.
38. Guo, Z., and Eisenberg, D. (2006) Runaway domain swapping in amyloid-like fibrils of T7 endonuclease I. *Proc. Natl. Acad. Sci. U.S. A. 103*, 8042–8047.
39. Lapatto, R., Nalini, V., Bax, B., Driessen, H., Lindley, P. F., Blundell, T. L., and Slingsby, C. (1991) High resolution structure of an oligomeric eye lens β-crystallin. Loops, arches, linkers and interfaces in βB2 dimer compared to a monomeric γ-crystallin. *J. Mol. Biol. 222*, 1067–1083.
40. Cho, S. S., Levy, Y., Onuchic, J. N., and Wolynes, P. G. (2005) Overcoming residual frustration in domain-swapping: The roles of disulfide bonds in dimerization and aggregation. *Phys. Biol. 2*, S44–S55.
41. Li, S., Schoneich, C., and Borchardt, R. T. (1995) Chemical instability of protein pharmaceuticals: Mechanisms of oxidation and strategies for stabilization. *Biotechnol. Bioeng. 48*, 490–500.
42. Chang, B. S., Beauvais, R. M., Arakawa, T., Narhi, L. O., Dong, A., Aparisio, D. I., and Carpenter, J. F. (1996) Formation of an active dimer during storage of interleukin-1 receptor antagonist in aqueous solution. *Biophys. J. 71*, 3399–3406.
43. Lou, M. F. (2003) Redox regulation in the lens. *Prog. Retinal Eye Res. 22*, 657–682.
44. Lofgren, S., Fernando, M. R., Xing, K. Y., Wang, Y., Kuszynski, C. A., Ho, Y. S., and Lou, M. F. (2008) Effect of thioltransferase (glutaredoxin) deletion on cellular sensitivity to oxidative stress and cell proliferation in lens epithelial cells of thioltransferase knockout mouse. *Invest. Ophthalmol. Visual Sci. 49*, 4497–4505.